THE INFLUENCE OF AQUIFER GEOCHEMISTRY ON SALT PRECIPITATION DURING CO_2 INJECTION: INSIGHTS FROM 1D SIMULATIONS USING THE RAND ALGORITHM

Fernando de A. Medeiros[1], Erling H. Stenby[1], Wei Yan[1*]

[1] Center for Energy and Resources Engineering, Department of Chemistry, Technical University of Denmark, 2800 Kongens Lyngby, Denmark

* Corresponding author e-mail: weya@kemi.dtu.dk

Abstract

CO_2 storage in saline aquifers is deemed as a feasible way to control the atmospheric levels of greenhouse gases. When CO_2 is injected in saline aquifers, several phenomena take place, such as multiphase fluid flow, adsorption and chemical reactions, which can in turn produce mineral phases that might risk the whole process. Thus, mathematical modelling of CO_2 storage in saline aquifers is a very complex task. In this work, we resort to the RAND algorithm for chemical and phase equilibrium (CPE), coupled with 1D material balance equations for multiphase fluid flow in porous media, to simulate the injection of CO_2 in saline aquifers. Two types of aquifers were studied: one with NaCl and water; and another one involving a more complex brine containing Na^+, Mg^{2+}, K^+, Cl^-, SO_4^{2-}. We focused the analysis on salt precipitation, a phenomenon that takes place when dry CO_2 is injected into an aquifer. From the 1D-simulation and from phase equilibrium diagrams, we produced insights on the thermodynamic conditions that allow for salt precipitation, the typical flow patterns observed, and the precipitation of multiple salts. The analysis performed is intended as a systematic evaluation of the interplay between geochemistry and fluid flow, with a special focus on salt clogging. Furthermore, we have shown the applicability of the RAND algorithm to challenging conditions involving fluid flow and several reactions and mineral phases.

Keywords: *Salt Precipitation, CO_2 storage, Saline Aquifers, Two-phase flow, Geochemistry*

1. Introduction

The underground storage (UGS) of CO_2 is an important means to control the atmospheric level of greenhouse effect gases [1]. One of the steps in the development of safe and efficient CO_2 UGS processes is the mathematical modeling of CO_2 injection into geological formations [2, 3, 4], such as saline aquifers, where CO_2 should remain trapped for long periods.

However, many phenomena take place when CO_2 mixes with brines and interact with minerals present in the geological formations [2], significantly increasing the complexity of the CO_2 UGS simulations. Among these phenomena, chemical and phase equilibria (CPE) play a central role, and, because of that, many geochemical simulators capable of performing CPE calculations exist in literature [5, 6, 7, 8]. Among those, there is the class of RAND algorithms. This type of method is a non-stoichiometric CPE algorithm, originally developed for problems at constant temperature and pressure [9, 10, 11]. We have recently applied a version of this algorithm (the modified RAND [12]) to problems involving CO_2, brine and minerals [13, 14]. Furthermore, we have coupled it with other algorithms to simulate conditions beyond thermodynamic equilibrium [15].

In this work, we coupled the RAND method with an algorithm for the 1D-simulation of two-phase flow in porous media, via the implicit solving of mass balance equations [16], and we performed simulations of CO_2 injection into saline aquifers containing brines. We studied two types of systems. First we studied a ternary system (NaCl, CO_2, H_2O), then we analyzed a complex brine (Na^+, Mg^{2+}, K^+, Cl^-, SO_4^{2-}). By doing so, we tested the robustness of the RAND algorithm and, from the results issued, we obtained insights on the evolution of the 1D reservoir under continuous CO_2 injection.

The analyses performed here were especially focused on the salt clogging problem. Salt clogging is generally considered a nuisance typical of CO_2 injection in saline aquifers [17]. Several phenomena may play a role in salt clogging (capillary effects, perpendicular flow, etc.). Its driving force, however, is related to geochemistry: the drying of the aquifer brine by constant mixing with a CO_2-rich stream. Salt clogging can lead to reductions in injectivity and ultimately render the whole storage procedure inefficient [17, 18]. Several simulation works capable of capturing salt precipitation or focusing on understanding the phenomenon are present in literature. They vary from analytical solutions to two-phase flow equations [19] to simulations involving multiple dimensions, capillary effects [20]. Here, we focus the analysis on the thermodynamic conditions that allow for salt clogging to occur, and we investigate the interplay between geochemistry and the 1D flow pattern observed.

2. Methodology

2.1 The modified RAND Algorithm

The modified RAND algorithm is a non-stoichiometric chemical and phase equilibrium algorithm first described

by Paterson et al. [12]. It has been previously tested with various systems (hydrocarbons [12, 21], CO_2 and minerals [13, 14], and petrochemicals [22]), and it has also been extended to equilibrium specifications other than T and P [23, 24, 25].

In this work, the RAND method for closed systems at fixed T and P was used as the phase equilibrium core of an implicit algorithm to solve the multiphase material balance equations in porous media. Figure 1 shows a schematic representation of the problem. The reservoir is divided into a finite number of cells and CPE calculations are performed in each one of them. As a consequence of this coupling, the precipitation reactions and the mixing between brine and CO_2 are considered equilibrated, i.e. instantaneous w.r.t the time scale of the simulation.

Furthermore, the RAND algorithm was utilized to generate the phase diagrams presented here (Figure 2, 14, and similar ones). A methodology similar to the reaction path analysis was used in those cases [15, 26], which consists in a stepwise addition of a given mineral. Then, a phase equilibrium calculation is performed at the new conditions to observe how the system responds to the mineral addition.

2.2 The 1D Simulation Algorithm

Multiphase flow into a 1D reservoir is described in this work by the following equation:

$$\phi\frac{\partial}{\partial t}\left(\sum_{j=1}^{N_F} x_{ij}\rho_j s_j\right)+\frac{\partial}{\partial x}\left(\nu\sum_{j=1}^{N_F} x_{ij}\rho_j f_j\right)=0 \tag{1}$$

in which ϕ represents the porosity of the reservoir, x_{ij} represents the molar fraction of component i in phase j, v represents the velocity of the fluid flow, ρ_j is the density of phase j, s_j is the saturation of phase j and f_j is the fractional flow function value of phase j. This equation is valid for all N_C components, and the summations in phase run until they reach the total number of fluid phases N_F. This equation can be made dimensionless by the introduction of dimensionless time (τ, measured in pore volumes injected, p.v.i.); dimensionless distance (χ) and dimensionless velocity (v_D). It becomes:

$$\frac{\partial G_i}{\partial \tau}+\frac{\partial F_i}{\partial \chi}=0 \tag{2}$$

with

$$G_i=\sum_{j=1}^{N_F} x_{ij}\rho_j s_j;\ F_i=\nu_D\sum_{j=1}^{N_F} x_{ij}\rho_j f_j \tag{3}$$

Equation (1) is obtained after the assumption of Darcy flow and the same value of pressure for all fluid phases. The solution of Equation (2) is self-similar, i.e., the solution for both τ and χ can be obtained from a single variable, the so-called similarity variable $\xi = \chi/\tau$. The fractional flow function f_j is obtained as

$$f_j=\frac{k_{r,j}/\mu_j}{\sum_{j=1}^{N_F} k_{r,j}/\mu_j} \tag{4}$$

with constant viscosities and relative permeabilities of a fluid phase j ($k_{r,j}$) calculated as in Yan et al. [16]. This equation is solved using the implicit algorithm described by Yan et al. [16]. In this algorithm, the fluid flow equation is solved separately from the CPE part. The effect of salt precipitation in our analysis is accounted for only in the porosity of a cell. The values of porosity reduction ($\phi/\ \phi_0$) presented here were calculated as a function of the volume of each solid phase k (V_k) and the volume of the cell (V_{cell}):

$$\frac{\phi}{\phi_0}=V_{cell}-\frac{\sum_{k=1}^{N_S} V_k}{V_{cell}} \tag{5}$$

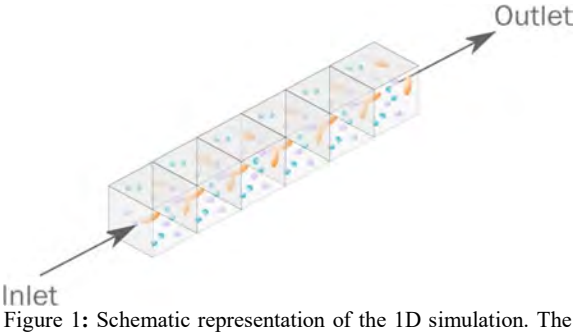

Figure 1: Schematic representation of the 1D simulation. The reservoir is split into different cells where the CPE calculations are performed. Flow from once cell to the other is taken into account by Equation 1.

Table 1: Simulation parameters.

Reservoir and Fluid Properties	**Value**
Residual saturation (brine)	0
Residual saturation (CO_2-rich fluid)	0
Viscosity brine / (Pa.s)	5×10^{-4}
Viscosity CO_2-rich fluid / (Pa.s)	1×10^{-4}
Temperature / K	328.15
Pressure / MPa	17.9
Numerical Scheme Properties	**Value**
Number of cells	300
Number of time steps	3000
Number of moles injected per time step	0.1
Total mole number in the initial cell	1

3. Results

3.1 Benchmark Simulation (NaCl + CO_2 + H_2O)

In the first set of results, we analyze the CO_2 addition to a reservoir containing NaCl and water. This simulation works as a benchmark for the rest of this study, as it establishes the main parameters and features of the 1D simulation. The results for the ternary system have three parts. First, we present the ternary diagram of the NaCl + CO_2 + H_2O system at the conditions of temperature and pressure used in the 1D simulations. From this initial analysis, we can identify all the possible thermodynamic states of the brine and the CO_2-rich fluid phase, and they can be interpreted as the underlying set of possible thermodynamic states in which the 1D simulation unfolds.

Second, we set an initial brine molality and the composition of the injected CO_2-rich fluid, and we show

how the fluid properties are distributed along the 1D-reservoir w.r.t. dimensionless time and space.

Third and finally, we analyze the interplay between the results observed in the first part and in the second part, i.e., the relation between the thermodynamic behavior of the system and the general aspect of fluid flow in the reservoir. By doing so, we were able to identify several typical zones in the 1D simulation.

3.1.1. The Ternary Diagram

The first system studied can be considered a ternary one ($NaCl + CO_2 + H_2O$), even though several reactions take place. The following reactions were considered in the aqueous phase:

$$H_2O_{(l)} \rightleftharpoons OH^-_{(aq)} + H^+_{(aq)} \quad (6)$$

$$CO^{2-}_{3,(aq)} + H^+_{(aq)} \rightleftharpoons HCO^-_{3,(aq)} \quad (7)$$

$$CO^{2-}_{3,(aq)} + 2\,H^+_{(aq)} \rightleftharpoons CO_{2,(aq)} + H_2O_{(l)} \quad (8)$$

The following interfacial reaction accounts for NaCl precipitation as a solid (halite):

$$Na^+_{(aq)} + Cl^-_{(aq)} \rightleftharpoons NaCl_{(halite)} \quad (9)$$

The parameters used to model the reactions were taken from PHREEQC's Pitzer database [5]. The CO_2-rich fluid phase was modeled by the PR equation of state [27] with binary interaction parameters set to zero. The Pitzer model [28], implemented as in Felmy and Weary [29], with interaction parameters from PHREEQC [5], was used for the brine. The density of the CO_2-rich fluid was obtained via PR-EoS, and the density of the brine was calculated using the approach of Apello et al. [30].

The application of the Gibbs phase rule to the system shows that the number of degrees of freedom (F) is a function of the number of components (N_C), number of phases (N_P), number of equilibrated reactions (N_R), number of phases containing ions (EL)

$$F = N_C - N_R - EL - N_P + 2 = 6 - N_P \quad (10)$$

However, Na^+ and Cl^- can only be added together as a single component and disappear from the brine as halite following the same stoichiometry. This has essentially added a constraint on the ratio between Na^+ and Cl^-, reducing F by 1, leading to a final value of $5 - N_P$. This means that if 3 phases are present at a fixed set of T and P, the system is completely determined. Furthermore, if 2 phases are present, there is only one degree of freedom left. In the single phase case, two extra intensive variables have to be specified to determine the state of the system. Thus, despite the large number of species present, this system can be virtually considered as a ternary one, as if no reaction or aqueous speciation was taken into account.

Figure 2 (a) shows the brine thermodynamic condition as a function of the molality (per kilogram of water) of NaCl and the total molality of carbonic species. The color scheme represents the tangent plane distance (*tpd*) [31] of halite (solid NaCl), and the dotted line represents its equilibrium with the brine. The tangent plane distance of a phase is a measure of its saturation. Below the dotted line (blue region), halite is undersaturated (positive *tpd*), and more NaCl has to be added to the brine before it reaches equilibrium. Above the dotted line (red region), halite is supersaturated (negative *tpd*), and it naturally precipitates from brines in these conditions. The solid black line represents the solubility of CO_2 in the brine. If the brine has a total CO_2 molality higher than the black line at a given molality of NaCl, it will eventually split into two phases, being the composition of the new CO_2-rich fluid phase given by Figure 2 (b). This figure represents the molar fraction of water (x-axis) in the CO_2-rich fluid phase, which consists only of H_2O and CO_2, in equilibrium with a brine of a certain molality of NaCl (y-axis). This means that a brine – Figure 2(a) – at the black line is in equilibrium with a fluid phase – Figure 2(b) – both at the same molality of NaCl. Furthermore, the interception between the dotted and the black line in Figure 2 (a) represents a ternary invariable point (at fixed T and P) containing NaCl, a brine and a CO_2-rich fluid, these two having their compositions established by Figure 2 (a) and (b), respectively.

3.1.2. Profiles along the Reservoir

We simulated the injection of a CO_2-rich fluid containing 0.001 of water (mole fraction) into an aquifer containing a brine of 2 molal NaCl (total 4 molal of dissolved Na^+ and Cl^- in water). The saturation and molality profiles at 0.576 p.v.i. are displayed in Figure 3.

3.1.3. Interplay between Simulation Zones and Thermodynamics

Figure 4 was obtained from the analysis of the saturation and molality profiles observed in all simulated values of p.v.i. for the whole reservoir. The x-axis of Figure 3

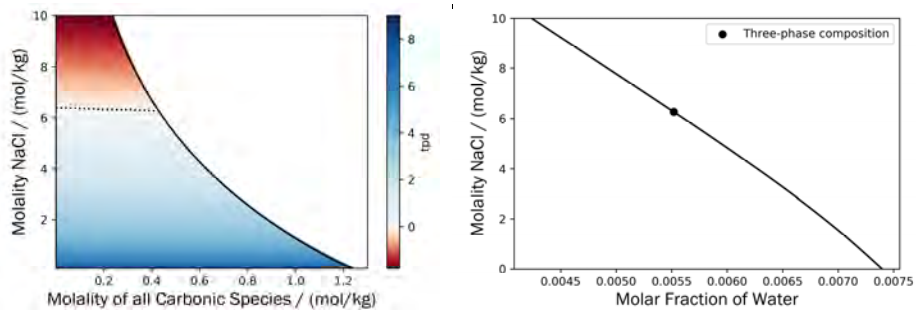

Figure 2: (a) Ternary phase diagram of the NaCl + CO_2 + H_2O system at 328.15 K and 176.659 atm; (b) composition of the CO_2-rich fluid in equilibrium with the brine depicted in (a).

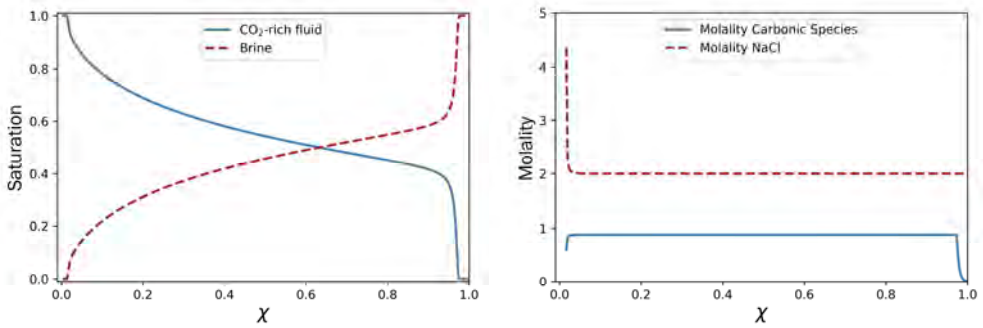

Figure 3: Saturation (a) and molality (b) profiles at 0.576 p.v.i.

(dimensionless distance) corresponds to the y-axis of Figure 4, and the x-axis of Figure 4 is the juxtaposition of the different time steps of the simulation (i.e. different values of p.v.i.). From Figure 4, we see that the simulation can be divided into five different zones. Zone A has just one phase and it corresponds to the unswept brine, i.e., the change in brine composition is not observable to the machine precision level. This zone should not appear in the analytical solution. Zone B corresponds to a one phase region containing a brine that has already undergone a composition change, but it is still not saturated in CO_2. This zone is characterized by a steep increase in CO_2 molality (Figure 3(b) close to χ=1). Zone C corresponds to the two-phase region containing both brine and the CO_2-rich fluid. In this zone, the saturation of the brine reduces, and we see a similar development to Figure 3 from close to χ=1 to close to χ=0. Zone D is very narrow and corresponds to a three-phase region. In this zone, precipitation of solid NaCl has already taken place and the brine drying is in its late stages. Since the equilibrium assumption is used in the simulation, this three-phase zone is very narrow and corresponds to just a single cell for a given time step, and it only moves forward in χ once the brine has evaporated completely. Finally, we have Zone E, which is the dry-out zone, containing halite and CO_2-rich fluid. This zone is characterized by a marked porosity reduction (around 0.4% at 3.46 p.v.i., Figure 5). Since the two phases present do not interact, no further changes w.r.t. the system variables occur in Zone E. The boundaries of the zones correspond to different fronts, whose velocities can be determined from Figure 4, as $\xi_F = \chi_F/\tau_F$. Hence, the state of a cell at a certain time (τ) and position (χ) can be inferred by comparison of dimensionless variable of the cell ($\xi = \chi/\tau$) to the front velocities.

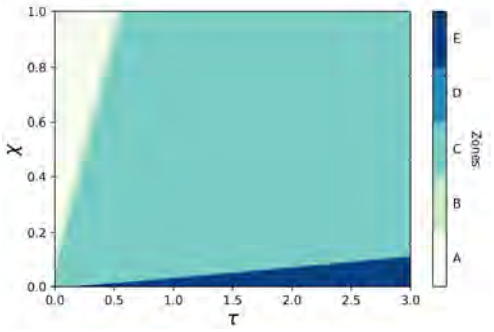

Figure 4: Different zones of the benchmark simulation w.r.t. space (χ) and time (τ).

The simulation can be better understood if we plot the different zones from Figure 4 in the ternary diagram. In Figure 6, one can see the thermodynamic state of every simulation cell over the ternary diagram from Figure 2 (a). Zone A corresponds to a dot in the y-axis marking the initial brine molality of 2 molal NaCl. As the fluid flow brings carbon-containing species to the brine, the thermodynamic state of the system moves almost as a straight line until it reaches the solubility limit of CO_2 (full black line).

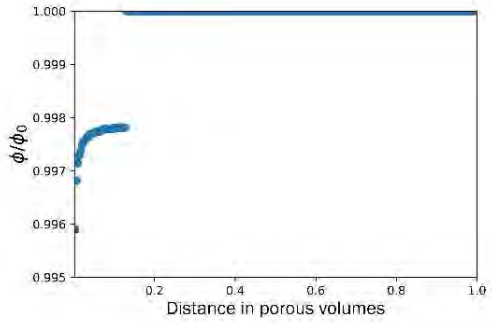

Figure 5: Porosity decrease w.r.t. to reservoir distance χ at 3.46 p.v.i. (benchmark simulation).

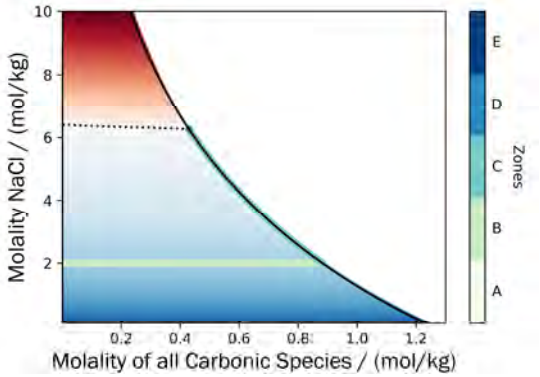

Figure 6: Thermodynamic path of the different zones of the benchmark simulation.

The pale green straight line connecting those two limits corresponds to the thermodynamic states within Zone B. As soon as the system reaches the solubility line of CO_2, it enters Zone C, which moves along the solubility line, until it reaches equilibrium with halite (the dotted line) and originates Zone D, containing three phases. Finally, Zone E cannot be represented in this plot, since the brine is no longer present. Figure 6 shows that some

characteristics of the 1D simulation can be inferred from a simple ternary diagram, including the thermodynamic path of the 1D simulation and the thermodynamic state of each cell at a certain pair of χ and τ.

3.2 Sensitivity Analysis: Injected Fluid Composition

Based on the analysis in Section 3.1, we proceed to analyze how the composition of the injected fluid affects the general behavior of the simulation. We selected three values of water composition in the CO_2-rich injected fluid (0.006, 0.007 and 0.01 in molar fraction) and compared their results to the benchmark one from section 3.1 (0.001). None of the three new simulations generated the same five zones as in the benchmark one. They produced only three zones, without any NaCl precipitation. No obvious changes were observed w.r.t. the front velocities.

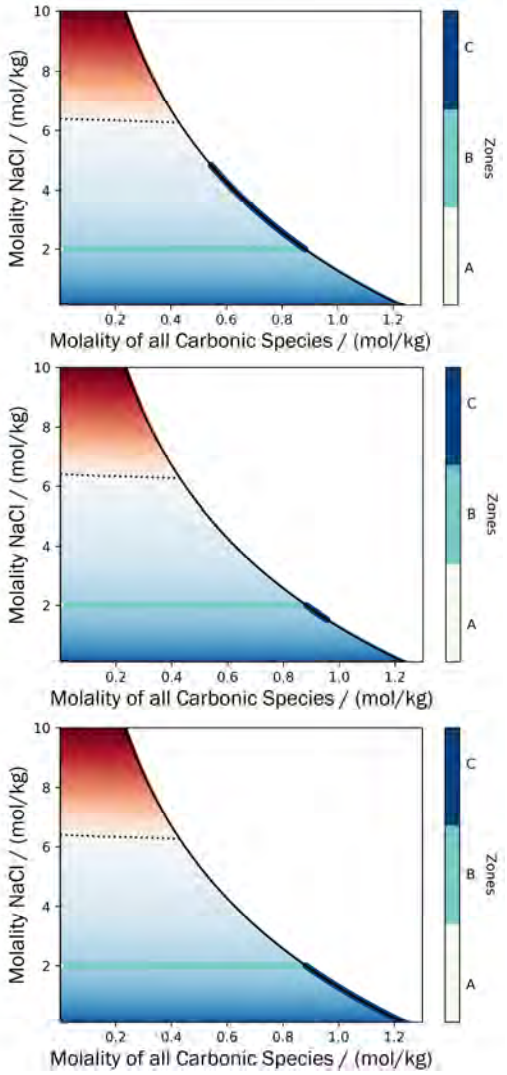

Figure 7**:** Thermodynamic path of the simulations with different compositions of the injected fluid: (a) 0.006 mole fraction of water; (b) 0.007 mole fraction of water; and (c) 0.01 mole fraction of water.

A better understanding of this behavior is obtained by analyzing the thermodynamic path (Figure 7). The CO_2-rich fluid composition plays a major role in the drying of the brine. The composition of 0.006 leads to brine concentration, which is not strong enough to ever reach salt precipitation – Figure 7 (a). The injection of compositions of 0.007 and 0.01 dilute the brine, the former stopping at a certain value of NaCl molality (Figure 7 (b)) and the latter washing out completely any solute in the brine (Figure 7 (c)).

The different thermodynamic paths can be explained by the composition of the CO_2-rich phase in equilibrium with the brine. Figure 8 shows four different ranges of wetness for the injected CO_2-rich phase at fixed T and P for an initial brine composition of 2 molal. Range W corresponds to the range of compositions that lead to salt clogging. They include all compositions dryer than the three-phase equilibrium composition (blue dot). Range X corresponds to a range of wetness that concentrates the brine, but stops until the brine reaches its equilibrium molality w.r.t. the injected fluid. This range encompasses compositions between the three-phase equilibrium one (blue dot) and the two-phase equilibrium at the molality of the initial brine (yellow dot). Range Y corresponds to a humid injection fluid, which dilutes the brine, until the brine reaches a molality in equilibrium with the injected fluid. The range is bounded by the two-phase equilibrium composition at the initial brine molality (yellow dot) and the CO_2 composition when in equilibrium with pure water (orange dot). Range Z represents a CO_2 stream which is supersaturated with water and washes out completely all solutes in the brine. All compositions higher than the composition of the CO_2-rich fluid in equilibrium with pure water belong to this range, i.e. CO_2 supersaturated with water. The saturation profiles at late stages of the simulation displayed in Figure 9 can give us an idea of how the fluid flow responds to the change in composition of the injected fluid. The composition of 0.001 (range W) leads to a sharp saturation front that reaches 1. The composition of 0.006 (range X) will eventually lead to the complete vanishing of the brine (s_g=1), but there is no sharp front or salt precipitation. The steep increase in saturation might be attributed to the reducing CO_2 solubility as the brine gets more concentrated in NaCl. The composition of 0.007 also eventually leads to the vanishing of the brine, without any salt precipitation. One can also see a slight tendency of decrease in the CO_2-rich fluid saturation, probably due to the increase in CO_2 solubility as the brine is diluted. Finally, the composition of 0.01 (range Z) does not lead to the vanishing of the brine. Rather, it tends to a saturation plateau around s_g=0.94. This is because the injected fluid is already saturated in water and an aqueous phase naturally appears. It follows from the analysis that the injected fluid composition that leads to salt precipitation is a function of the geochemistry of the system (i.e., T, P and initial brine composition), and the saturation profiles observed are a function of the possible thermodynamic states of the system.

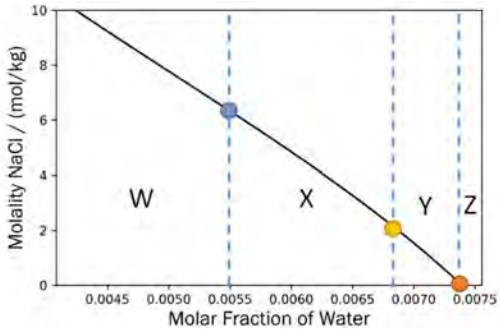

Figure 8: Different water fraction regions in the injection fluid for a brine at 2 molal NaCl.

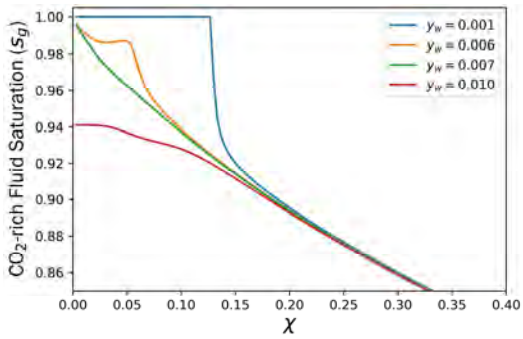

Figure 9: Typical saturation profiles according to the composition of the injected fluid.

3.3 Sensitivity Analysis: Initial Brine Molality

The initial molality of an aquifer brine has been regarded as one of the most important parameters in the salt clogging phenomenon [17]. Here, we have performed a sensitivity analysis by selecting two different initial brine molalities (4 and 6 molal of NaCl) and we compared it to the benchmark one (2 molal).

No major changes were observed in the overall results of the simulation. The same five zones (A, B, C, D and E) are present, with some minimal changes to their front velocities. The variable that was most influenced by the change in molality was porosity. Higher values of molality result in larger porosity reductions, as seen in Figure 10, in comparison to the benchmark one (Figure 5). The molalities of 2, 4 and 6 led to maximum porosity reductions of around 0.4%, 0.8%, 1.4%, respectively. Even though the porosity changes are not large, it has been shown that even minor changes in porosity can lead to important reductions in permeability [17, 18], which the simulations we have performed here were not capable of capturing. In addition, the simulations were performed at residual saturations of 0 for both the brine and the CO_2-rich fluid and, therefore, the reduction might be more drastic in real cases.

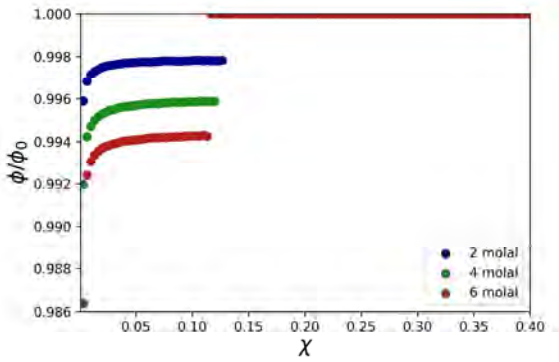

Figure 10: Porosity decrease w.r.t. to reservoir distance χ at 3.46, 3.40 and 3.31 p.v.i. for initial brine molality of 2, 4 and 6 molal of NaCl, respectively.

3.4 Analysis of a Complex Brine

In this part, we apply the methodology we have discussed for the NaCl + CO_2 + H_2O system to a more complex brine containing the following mole ratio of elements: 0.4 Na^+, 0.002 K^+, 0.02 Mg^{2+}, 0.44196 Cl^- and 0.00002 SO_4^{2-}. All parameters needed were taken from the Pitzer database from PHREEQC [5]. Many solids can precipitate from it. The construction procedure of the pseudo-ternary phase diagram (Section 3.4.1) allowed for the precipitation of all available minerals in PHREEQC that involve the five ionic species mentioned. After the identification of the ones that actually precipitated, the list of possible minerals was shortened to four: halite, carnallite, bischoffite and kieserite.

3.4.1. The Pseudo-Ternary Diagram

As in the previous case, we performed here a reaction path analysis [13, 26], using the RAND algorithm. The complex brine has several anions and cations, but the system can still be represented in a ternary manner, as

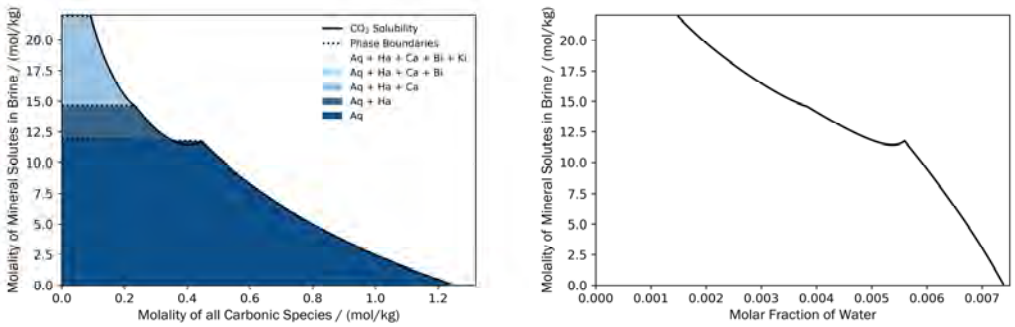

Figure 11: (a) Pseudo-ternary phase diagram of the complex brine; (b) Composition of the CO_2-rich fluid in equilibrium with the brine from (a).

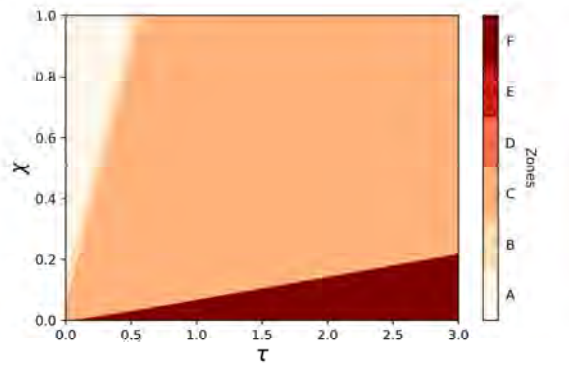

Figure 12: Different zones of the real brine simulation w.r.t. space (χ) and time (τ) (analogous to Figure 4).

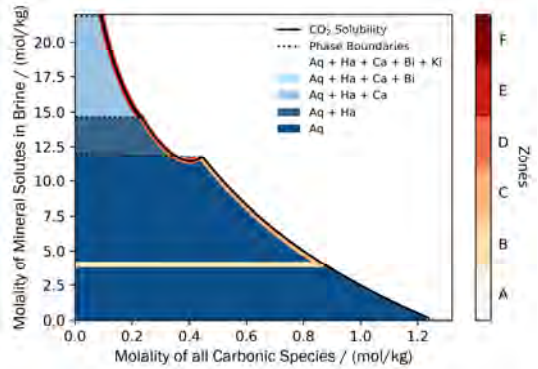

Figure 13: Thermodynamic path of the different zones of the real brine simulation (analogous to Figure 6).

only the amount of carbonic species and water changes due to CO_2 injection and drying. However, now, several different minerals can precipitate and they follow a certain order of appearance w.r.t. to the drying of the brine. The mineral composition of the whole system (solid phases included) does not change, but once precipitation of a given salt starts, the mineral proportions in the brine change. In Figure 11 (a) we see the pseudo-ternary diagram of the complex brine. There is a region at lower molalities in which only an aqueous phase (Aq) is present. As the molality increases, the system crosses the first phase boundary (dotted line) and halite (Ha) precipitates. From this point onwards, the mineral proportions in the brine no longer correspond to the global one. As water is further removed, carnallite (Ca) precipitates, followed by Bischoffite (Bi) and Kieserite (Ki), ending in a very small 5-phase region. The solid black line represents the solubility of CO_2 in the brine phase. Figures 11 (b) shows the water molar fraction of the CO_2-rich fluid (x-axis) in equilibrium with a mineral system of molality given by the y-axis.

3.4.2. The Flow Variables and the Different Zones in a Complex Brine

The 1D simulation results are presented in Figure 12. In the NaCl example, 5 zones were present. Here, 6 zones were observed. Zone A, B and C have the same meaning as before, i.e., unswept brine, zone of molality increase in CO_2 in the single phase, and two-phase flow, respectively. Zone D represents the precipitation of halite and it is immediately followed by Zone E, which is a four-phase zone (brine, CO_2-rich fluid, halite and carnallite). Since the amounts of bischoffite and kieserite are very small, no precipitation front for those two phases was observed. They only appeared in the dry-out zone (Zone F), which here consists of the CO_2-rich fluid, halite, carnallite, bischofite and kieserite. Regarding the front velocities of the different zones, we see no major changes w.r.t. to Zone A, B and C, when compared to the NaCl benchmark case (Figure 4). Halite precipitation front, however, is faster here than it was before (2/30 > 1/30), even though the molality of total solutes in water was the same at the beginning of the simulation (4 molal of dissolved ions), and this is probably due to a decrease in halite solubility in the presence of other solutes (salting out effect). From Figure 11 (a), we see that halite starts precipitating at around 12 molal of total dissolved ionic species (6 molal of NaCl, i.e., 6 molal of Na^+ and 6 molal of Cl^-), whereas in the real brine it starts around 11 molal.

The plotting of the simulation zones on top of the pseudo-ternary diagram (Figure 13) reveals the regions that are hard to see in Figure 12. Zone A is again a dot in the y-axis marking the initial brine molality. As CO_2 is added to the brine, a straight line appears until the system achieves CO_2 solubility (Zone B). The system moves along the solubility line until halite precipitates (Zone C). After halite precipitation, there is a major change in the solubility curve and the system enters Zone D. Zone D goes on until carnallite precipitates, at the beginning of Zone E. Zone F is not plotted in the diagram, as the brine has evaporated completely.

The porosity profile at 3.55 pvi reveals an increase in porosity reduction when compared to the benchmark simulation (Figure 14). There are two main causes for this. One is that more halite (the major constituent of the complex brine) precipitates as its solubility is reduced and the other one is the higher molar volumes of the other mineral phases, especially carnallite, the second most abundant mineral. In addition, the plot presents several numerical fluctuations. This is probably because the trace amounts of kieserite and bischoffite are close to machine precision.

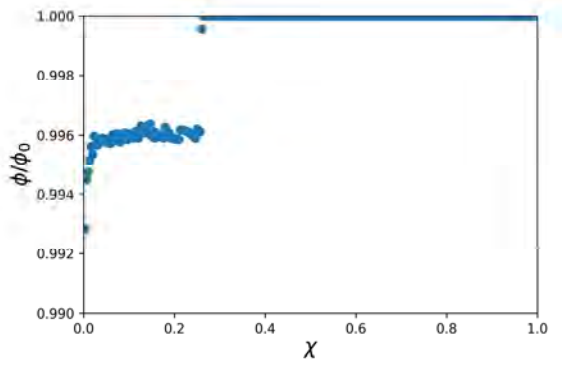

Figure 14: Porosity decrease w.r.t. reservoir distance (χ) at 3.55 p.v.i. (complex brine).

4. Conclusions

In this work, we have successfully coupled the RAND CPE algorithm with an implicit solver for the 1D material balance equations governing the two-phase flow in porous media (Equation 1) and from those simulations, we obtained insights on the relation between geochemistry and fluid flow in a saline aquifer.

The results show that the core equilibrium algorithm is robust and suitable for compositional simulation. It was tested under challenging conditions, with many phases present, both solid and fluid. The algorithm also succeeded in calculating the precipitation of minerals present at very small amounts in the brine and the results are sound from a geochemical perspective.

The results for the NaCl + CO_2 + H_2O and for the complex brine provide a systematic approach to assess salt clogging conditions in different formation waters. From this simple analysis, we can infer the composition of the injected fluid that lead to precipitation, the most important features of fluid flow, the different mineral phases that can appear, and the relation between fluid flow and geochemistry.

Acknowledgment

The study was carried out under "modelling of CO_2 induced near wellbore precipitation phenomena" funded by Energy Cluster Denmark.

References

[1] IPCC Special Report on Carbon Dioxide Capture and Storage, Technical Report, IPCC, 2005.

[2] X. Jiang, A review of physical modelling and numerical simulation of long-term geological storage of CO_2, Applied Energy 88 (2011) 3557–3566.

[3] A. N. J. Bear, J. Bensabat, Geological Storage of CO2inDeepSalineFormations, volume 29, 2017.

[4] P. Liu, T. Zhang, S. Sun, A tutorial review of reactive transport modeling and risk assessment for geologic CO2 sequestration, Computers and Geosciences 127 (2019) 1–11.

[5] D. L. Parkhurst, C. A. J. Appelo, Description of input and examples for PHREEQC version 3:a computer program for speciation, batch-reaction, one-dimensional transport, and in-verse geochemical calculations, Technical Report, Reston, VA, 2013.

[6] T. J. Wolery, EQ3/6, a Software Package for Geochemical Modeling of Aqueous Systems, Technical Report, Lawrence Livermore National Lab., Livermore, CA, 1992

[7] D. A. Kulik, T. Wagner, S. V. Dmytrieva, G. Kosakowski, F. F. Hingerl, K. V. Chudnenko, U. R. Berner, GEM-Selektor geochemical mod-eling package: Revised algorithm and GEMS3K numerical kernel forcoupled simulation codes, Computational Geosciences 17 (2013) 1–24.

[8] T. Xu, N. Spycher, E. Sonnenthal, TOUGHREACT User's Guide: A Simulation Program for Non-isothermal Multiphase Reactive Transport in Variably Saturated Geologic Media, version 2.0, Technical Report October, Earth Sciences Division, Lawrence Berkeley National Laboratory, Berkeley, CA, 2004.

[9] S. R. Brinkley, Calculation of the equilibrium composition of systems ofmany constituents, The Journal of Chemical Physics 15 (1947) 107–110.

[10] W. B. White, S. M. Johnson, G. B. Dantzig, Chemical equilibrium incomplex mixtures, The Journal of Chemical Physics 28 (1958) 751–755.

[11] H. Greiner, An efficient implementation of newton's method for complex nonideal chemical equilibria, Computers and Chemical Engineering 15(1991) 115–123.

[12] D. Paterson, M. L. Michelsen, E. H. Stenby, W. Yan, New formulations for isothermal multiphase flash, Society of Petroleum Engineers - SPE Reservoir Simulation Conference 2017 (2017) 1947–1964.

[13] F. d. A. Medeiros, E. H. Stenby, W. Yan, RAND-Based Geochemical Equilibrium Algorithms with Applications to Underground Geological Storage of CO2, submitted to Advances in Water Resources (2021).

[14] C. Tsanas, E. H. Stenby, W. Yan, Calculation of multi-phase chemical equilibrium in electrolyte solutions with non-stoichiometric methods, Fluid Phase Equilibria 482 (2019)81–98.

[15] F. d. A. Medeiros, W. Yan, E. Stenby, Modified RAND Algorithms for Multiphase Geochemical Reactions, in: ECMOR XVII, European Association of Geoscientists & Engineers, 2020, pp. 1–15.

[16] W. Yan, M. L. Michlesen, E. H. Stenby, Calculation of minimum miscibility pressure using fast slimtube simulation, Proceedings - SPE Symposium on Improved Oil Recovery 1 (2012) 386–401.

[17] R. Miri, H. Hellevang, Salt precipitation during CO2 storage-A review, International Journal of Greenhouse Gas Control 51 (2016)136–147.

[18] Y. S. Jun, D. E. Giammar, C. J. Werth, Impacts of geochemical reactions on geologic carbon sequestration, Environmental Science and Technology 47 (2013) 3–8.

[19] M. Noh, L. W. Lake, S. L. Bryant, A. Araque-Martinez, Implications of coupling fractional flow and geochemistry for CO2 injection in aquifers, SPE Reservoir Evaluation and Engineering 10 (2007) 406–414.

[20] L. André, Y. Peysson, M. Azaroual, Well injectivity during CO2storage operations in deep saline aquifers - Part 2: Numerical simulations of drying, salt deposit mechanisms and role of capillary forces, International Journal of Greenhouse Gas Control 22 (2014)301–312.

[21] D. Paterson, W. Yan, M. L. Michelsen, E. H. Stenby, Multiphase isenthalpic flash: General approach and its adaptation to thermal recovery of heavy oil, AIChE Journal 65 (2019) 281–293.

[22] C. Tsanas, E. H. Stenby, W. Yan, Calculation of Multiphase Chemical Equilibrium by the Modified RAND Method, Industrial and Engineering Chemistry Research 56 (2017) 11983–11995.

[23] D. Paterson, Flash Computation and EoS Modelling for Compositional Thermal Simulation of Flow in Porous Media, Springer Theses, Springer International Publishing, 2019.

[24] D. Paterson, M. L. Michelsen, W. Yan, E. H. Stenby, Extension of modified RAND to multiphase flash specifications based on state functions other than (T,P), Fluid Phase Equilibria 458 (2018)288–299.

[25] F. d. A. Medeiros, E. H. Stenby, W. Yan, State function-based flash specifications for open systems in the absence or presence of chemical reactions, AIChE Journal 67 (2021).

[26] L. Marini, Geological Sequestration of Carbon Dioxide: Thermodynamics, Kinetics, and Reaction Path Modeling, 1st ed., Elsevier, 2007.

[27] D.-Y. Peng, D. B. Robinson, A New Two-Constant Equation of State, Industrial & Engineering Chemistry Fundamentals 15 (1976)59–64.

[28] K. S. Pitzer, Thermodynamics of Electrolytes. I. Theoretical Basis and General Equations, The Journal of Physical Chemistry 77 (1973) 268–277.

[29] A. R. Felmy, J. H. Weare, The prediction of borate mineral equilibria in natural waters: Application to Searles Lake, California, Geochimica et Cosmochimica Acta 50 (1986) 2771–2783.

[30] C. A. Appelo, D. L. Parkhurst, V. E. Post, Equations for calculating hydrogeochemical reactions of minerals and gases such as CO2 at high pressures and temperatures, Geochimica et Cosmochimica Acta 125 (2014) 49–67.

[31] Michelsen, M. L., The isothermal flash problem. Part I. Stability, Fluid Phase Equilibria, 9 (1982) 1–19.